Materials Transactions, Vol. 48, No. 8 (2007) pp. 2094 to 2099
Special Issue on Thermoelectric Conversion Materials III

Thermoelectric Properties and Phase Transition of $(Zn_xCu_{2-x})V_2O_7$

Kotaro Sotojima[1,*1], Ryosuke O. Suzuki[2,*2], Koji Amezawa[1,3,*3] and Yoichi Tomii[1]

[1]*Department of Energy Science and Technology, Graduate School of Energy Science, Kyoto University, Kyoto 606-8501, Japan*
[2]*Department of Material Science, Graduate School of Engineering, Hokkaido University, Sapporo 060-8628, Japan*
[3]*Graduate School of Human and Environmental Studies, Kyoto University, Kyoto 606-8501, Japan*

The phase stability and thermoelectric properties of the layered structure of $(Zn_xCu_{2-x})V_2O_7$ solid solutions were studied for $x \geq 0.2$. X-ray diffraction measurements, compositional studies, and thermal analysis verified that the low-temperature form of the $(Zn_xCu_{2-x})V_2O_7$ solid solution (monoclinic structure, C2/*c*) was stable for $0.2 \leq x \leq 2$ when heated below 863 K in air. On heating, phase transformation occurred at least at $0.2 \leq x \leq 2$ at a nearly constant temperature of approximately 873 K; above this temperature, a high-temperature form of the $(Zn_xCu_{2-x})V_2O_7$ solid solution was formed.

The Seebeck coefficients of the low-temperature $(Zn_xCu_{2-x})V_2O_7$ solid solution exhibited large negative values in the range of approximately -520 to $-700\,\mu V/K$, and the electrical resistivity increased with Zn addition. The maximum power factor of 1.99×10^{-7} W/m K^2 was obtained at 823 K for the low-temperature form of the $(Zn_{0.2}Cu_{1.8})V_2O_7$ solid solution. [doi:10.2320/matertrans.E-MRA2007856]

(Received November 20, 2006; Accepted April 14, 2007; Published June 6, 2007)

Keywords: *Seebeck coefficient, electrical resistivity, vanadium oxide, phase diagram, layered structure*

1. Introduction

The layered structures of oxides show interesting electric behaviors such as superconductivity and thermoelectricity. Good thermoelectric properties can be obtained in complex oxides (*e.g.*, $Na_xCo_2O_4$) since their crystal structure have layered unit cells.[1–3] In a vanadium oxide system, a layered structure consisting of a chain of tetrahedral VO_4 units has been reported and it exhibits interesting magnetic properties.[4–6] The basic screw chains of VO_4 and its layered structure can also be seen in transition metal pyrovanadates, $M_2V_2O_7$ (M is a 3d-transition metal and V = V^{5+}).

For example, as shown in Fig. 1, the orthorhombic α-$Cu_2V_2O_7$ is described by layers comprising square planar bipyramid (Cu/ZnO_5) units, which are aligned in a zigzag manner along the *a* axis.[5,7–9] The layer is connected by three layers composed of tetrahedral (VO_4) units with analogous chains along the *b*-axis. Note that the metallic element (Cu) is located among the VO_4 layers. Both $Zn_2V_2O_7$ and $Cu_2V_2O_7$ have two crystal structures: low- and high-temperature phases. It is noteworthy that α-$Zn_2V_2O_7$ and β-$Cu_2V_2O_7$ commonly have a β-thortveitite structure (monoclinic, C2/*c*), which also contain the VO_4 units.[7–11] The displacement of VO_4 units is not so large that the monoclinic structure (Fig. 1(b)) can be approximated by a parallelogram, as shown in Fig. 1(a).[5,7,12] Although the electronic density of states (DOS) is not evident in these structures, the layer of Cu/ZnO_5 units is expected to become electronically conductive because the strong bonding of the layers of VO_4 units localizes the electrons of V and oxygen.

Nord and Stefanidis[13] reported that 35% of the Zn sites in monoclinic α-$Zn_2V_2O_7$ can be replaced by Cu atoms at 873 K. Schindler and Hawthorne[9] reported the existence of a complete solid solution between α-$Zn_2V_2O_7$ and β-$Cu_2V_2O_7$ at 1023 K. Because the replacement of the metal sites by Cu and Zn in the monoclinic structure of α-$Zn_2V_2O_7$/β-$Cu_2V_2O_7$ monotonically but anisotropically modifies the layer distance and the lattice constants,[5,8,9] the DOS at the Fermi level will be modified by this compositional change and a good value of the Seebeck coefficient can be expected.

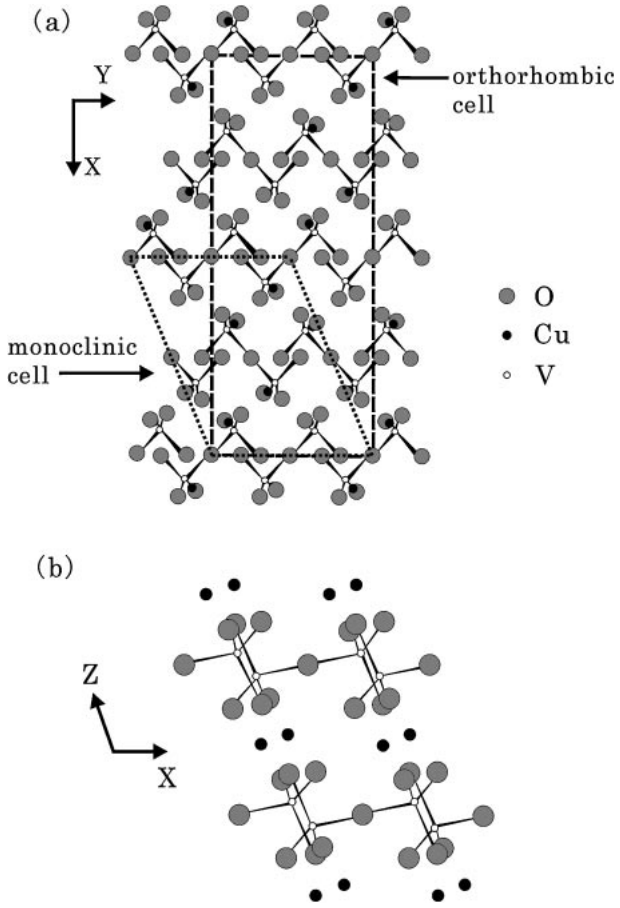

Fig. 1 Crystal structures of (a) orthorhombic α-$Cu_2V_2O_7$ and (b) monoclinic β-$Cu_2V_2O_7$.[5,7–13]

*1Graduate Student, Kyoto University
*2Corresponding author, E-mail: rsuzuki@eng.hokudai.ac.jp
*3Present address: Graduate School of Environmental Studies, Tohoku University

Therefore, the layered material suitable for thermoelectric conversion might be fabricated at a particular composition of the solid solution. A part of the strongly localized electrons inside the VO_4 units would be expected to provide the Cu/ZnO_5 layer with conductive electrons or holes by a structural distortion due to the substitutional replacement of the Cu/Zn sites or by the thermal vibration.

The purpose of this study is to investigate the thermoelectric properties of $Zn_2V_2O_7$, $Cu_2V_2O_7$, and their $(Zn_xCu_{2-x})V_2O_7$ solid solution. We found that the monoclinic structure of this solid solution transformed into a higher-temperature form; therefore, the thermal stability of the $(Zn_xCu_{2-x})V_2O_7$ solid solution was also studied using a thermal analysis and high-temperature X-ray diffraction (HT-XRD) measurements.

2. Experimental Procedures

Highly pure ZnO, CuO, and V_2O_5 powders were well mixed to yield nominal compositions of $Zn_2V_2O_7$ and $Cu_2V_2O_7$, and they were sintered twice in air below their melting temperatures[13,14] with several intermitted grindings. These two samples were mixed in a composition of $(Zn_x$-$Cu_{2-x})V_2O_7$ $(0 < x < 2)$ and sintered in the same manner. The pellets (diameter: 15 mm) were then sintered in vacuum in a graphite crucible by means of spark plasma sintering (SPS)[15,16] at 823 K for 1.2 ks under a mechanical pressure of 30 MPa. Subsequently, the pellets were again annealed at 823 K for 172.8 ks in air and cooled in the furnace.

The phases in these annealed samples were identified by powder X-ray diffraction (XRD) measurements using Cu Kα radiation. The phase constitutions and their metallic compositions were analyzed by scanning electron microscopy (SEM) equipped with energy dispersive X-ray spectrometry (EDX). The phase transition at high temperatures were analyzed in air by thermogravimetry (TG) and differential thermal analysis (DTA) using alumina crucibles at normal heating and cooling rates of 1/12 K/s and 1/60 K/s, respectively. The high-temperature phases were identified by XRD at room temperature in the cooled samples, and they were also monitored *in situ* in air by HT-XRD measurements using direct heating on a platinum sample stage and Mo Kα radiation.[17,18]

The Seebeck coefficient α and electrical resistivity ρ were measured in air between room temperature and 923 K using platinum lead wires and Pt-Pt13%Rh thermocouples.[19] The maximum temperature difference during the α and ρ measurements was suppressed to within 10 K and 1.0 K, respectively. The thermal conductivity, κ, was measured by the hot-disk method (TPA-501, Kyoto Electronics Manufactureing Co. Ltd.) at room temperature.

3. Results and Discussion

3.1 Sample preparation

When the oxide mixture was melted in an alumina crucible in air, the solidified sample in the crucible was wet and the constituent elements were not homogeneously distributed because of the formation of large dendrites during solidification. Even after annealing the solidified sample for a long time at 1003 K (below their melting temperatures), this inhomogeneous structure did not improve. This disagreed with the previous study that a solid solution was obtained at 1023 K after cooling from 1273 K.[9] When the oxide mixture was sintered at 823 or 1003 K in air for a longer duration (without melting), some pellets were very brittle, particularly for $x \geq 1.5$, and they could not be used in the thermoelectrical measurements. Therefore, after sintering in air, all the samples were grinded, pressed into pellets again, and sintered in vacuum by means of SPS. These SPS-sintered samples were sufficiently tough for the measurements. In order to confirm that equilibrium was attained in air at 823 K, all the SPS-sintered pellets were again annealed in air. These samples were not contaminated by carbon and alumina from the crucibles, and they were used for the following analysis.

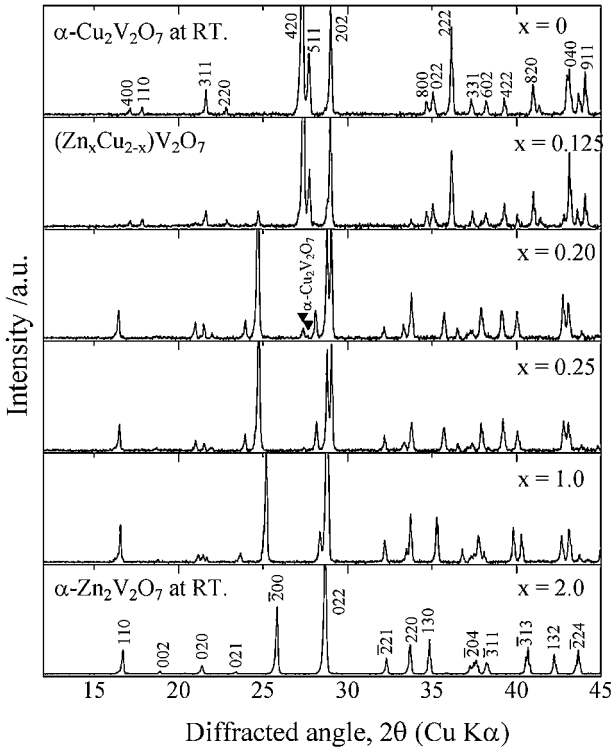

Fig. 2 XRD patterns at room temperature.

3.2 Low-temperature form of the $(Zn_xCu_{2-x})V_2O_7$ solid solution

Figure 2 shows some of the XRD patterns of the above-mentioned samples (measured at room temperature). The identified phases of all the samples are listed in Table 1, which were analyzed by the complemental information obtained from the SEM-EDX analysis. A mixture of two phases was obtained at $x \leq 0.2$, probably because of a short annealing time or a possible phase transition, while a homogeneous solid solution with a monoclinic structure (similar to β-$Cu_2V_2O_7$ and α-$Zn_2V_2O_7$) was obtained at $x > 0.2$. Therefore, $x > 0.2$ was particularly investigated in this study. The measured diffraction peaks monotonically changed their angles and intensities with the composition x for $x > 0.2$. The monoclinic lattice of pure α-$Zn_2V_2O_7$ with the space group C2/c ($\beta = 111.40°$, $a = 0.74367$ nm, $b = 0.83306$ nm, and $c = 1.01000$ nm[10]) was obtained for index-

Table 1 Identified phases of $(Zn_xCu_{2-x})V_2O_7$ samples at room temperature annealed at 823 K in air and their compositional analysis.

Nominal composition, x	Phases identified by XRD	Composition analyzed by SEM-EDX (mol%)		
		Zn	Cu	V
0.0	α-CuV_2O_7	—	46.2	53.8
0.15	α-CuV_2O_7 + LT ss			
0.2	α-CuV_2O_7 + LT ss	4.6	42.8	52.6
0.25	LT ss	5.6	41.6	52.7
0.5	LT ss	11.5	35.1	53.4
0.75	LT ss			
1.0	LT ss	23.2	23.0	53.8
1.25	LT ss			
1.5	LT ss	34.4	12.0	53.6
1.75	LT ss			
2.0	α-$Zn_2V_2O_7$	45.7	—	54.3

LT ss: low-temperature form of the $(Zn_xCu_{2-x})V_2O_7$ solid solution with a monoclinic structure.

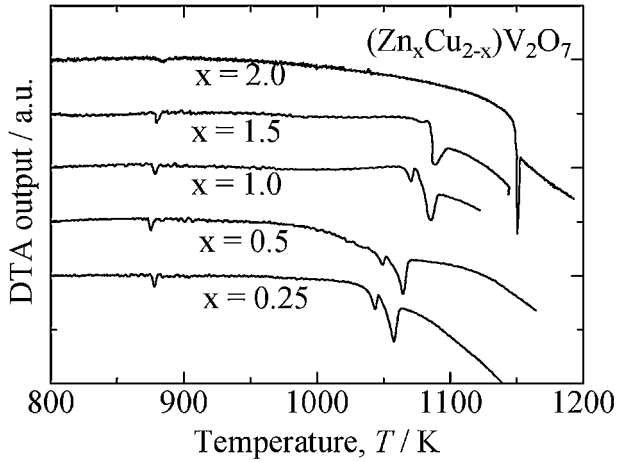

Fig. 3 DTA curves of $(Zn_xCu_{2-x})V_2O_7$.

ing *hkl*. Earlier reports[8,11,20–22] are in good agreement with recently obtained values.[10]

Although the precipitation of the second phase such as $Cu_{11}O_2(VO_4)_6$,[8] CuV_2O_6,[14,23] and $Cu_3V_2O_8$[14] was often reported, it has never been found in XRD, SEM and EDX analysis for $x > 0.2$. The analytical compositions observed by EDX exhibited marginally greater vanadium concentrations than those of the nominal compositions, as shown in Table 1, although the molar ratios of Zn and Cu matched well with the nominal compositions. If an experimental error of a few % in vanadium in the EDX analysis is permitted, we might conclude that these analytical values are in good agreement with the nominal compositions. Hereafter, this solid solution is referred to as LT ss (low-temperature form of the $(Zn_xCu_{2-x})V_2O_7$ solid solution) and x denotes the nominal composition of Zn.

Figure 3 shows the DTA heating curves of the annealed samples. The samples ($x > 0.2$) were melted above 1046 K with single or double endothermic peaks. The phase transition from the LT ss to a high-temperature phase was recorded as the smaller endothermic peak at approximately 873 K. The phase transition temperatures were nearly constant at 873 K for $x > 0.2$. The onset temperatures of these peaks for all the measured samples are shown in Fig. 4.

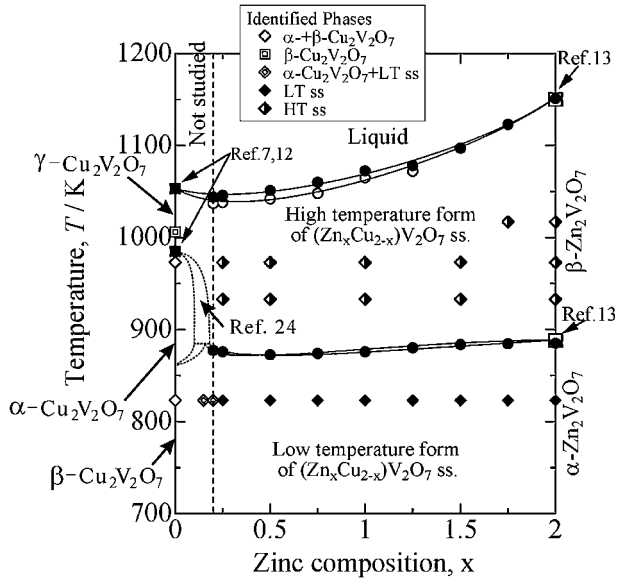

Fig. 4 Onset temperatures obtained from DTA curves (open and closed circles), and phase identification by XRD at room temperature and HT-XRD.

It was reported that a phase transition in $Cu_2V_2O_7$ occurred at 985 K and it melts at 1053 K;[7,12,14] further, monoclinic α-$Zn_2V_2O_7$ transforms into β-$Zn_2V_2O_7$ at 888 K and it melts at 1150 K.[13] The temperatures obtained in earlier studies agree with the DTA data shown in Fig. 4.

Because the endothermic reaction due to the phase transition was small, it was difficult to distinguish the details from the DTA curves. For example, a two-phase region should exist in a temperature range near 873 K at $0.25 \leq x \leq 2$ (between the stable regions of the high- and low-temperature forms of $(Zn_xCu_{2-x})V_2O_7$ solid solutions); however, this region was not clearly visible in the DTA data. Mass changes occurring during the phase transitions on heating were analyzed by means of TG; however, little changes were observed at the solid–solid phase transitions in all the samples for $0.25 \leq x \leq 2$. We concluded that neither oxidation nor reduction occurs at the phase transitions between the low- and high-temperature phases.

A significant mass loss was, however, found in some samples ($x < 1$) upon melting; phases that were not found in the quasi-binary systems of $Cu_2V_2O_7$ and $Zn_2V_2O_7$ were observed in the solidified samples. The two endothermic peaks can be attributed to the oxygen loss and melting, and the endothermic reactions can be attributed to the oxygen pressure in the ambient atmosphere. Therefore, Fig. 4 only shows a possible scheme of the quasi-binary phase diagram in air below the temperature at which melting and oxide reduction initiates. A detailed study on the phase diagram will be separately reported by including the data for $x < 0.25$.[24]

The solid solubility ($0.25 \leq x \leq 2$) obtained at 823 K was greater than that obtained by Nord and Stefanidis ($1.3 \leq x \leq 2$).[8] Their maximum solubility of Cu in α-$Zn_2V_2O_7$ ($x = 1.3$) was reported on the basis of the sample

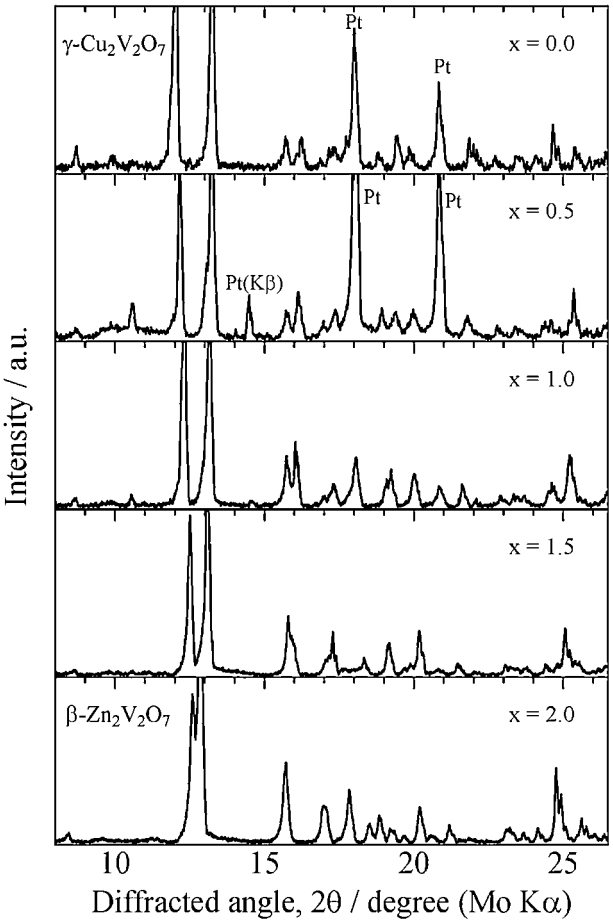

Fig. 5 HT-XRD patterns above the phase transition temperature.

annealed at 873 K, which is very similar to the phase transition shown in Fig. 4. Their report can be verified by considering the formation of a high-temperature phase in their samples at $x < 1.3$. Thus, their report is in good agreement with our tentative phase diagram shown in Fig. 4.

3.3 High-temperature form of $(Zn_xCu_{2-x})V_2O_7$ solid solution

The single phase of the high-temperature form could not be quenched to room temperature by several rapid cooling attempts after maintaining it at a constant temperature above 873 K. During cooling, the color of the Cu-rich sample changed from black to violet or red, while that of the Zn-rich sample changed from dark yellow to pale yellow. Some portions of the sample might maintain their high-temperature form even at room temperature immediately after quenching, but the color of the sample rapidly changed. The high-temperature form also rapidly decomposed during the XRD measurement at room temperature. The phase transition from the LT ss to the high-temperature phase, however, could be monitored by the HT-XRD, where the samples were rapidly heated (about 30 K/s) and maintained at a constant temperature.

Figure 5 shows the HT-XRD patterns above the phase transition temperature. The pattern at $x = 2.0$ matches with those of β-$Zn_2V_2O_7$,[13] while the pattern at $x = 0.0$ could not be explained by the reported patterns of α-$Cu_2V_2O_7$.[7,25] This is partially because the diffraction lines located closely could not be separated because of the low resolution of HT-XRD due to thermal vibration, while the reported patterns were measured at room temperature. Our separated study reports the formation of γ-$Cu_2V_2O_7$.[24]

The diffracted angles and intensities of the measured diffraction lines changed monotonically with x at $x > 0.2$. For example, the overlapped peaks at 13.01° and 13.29° for $x = 2.0$ were completely split into two peaks at $x < 2$, as shown in Fig. 5; they were more widely separated at $x < 1$. Therefore, the phases identified by the HT-XRD analysis at the studied compositions and temperatures are shown in Fig. 4. The continuous shift of the diffraction peaks indicates that the high-temperature form of the solid solution existed stably at least between $x = 0.2$–2.0. Hereafter, this solid solution will be referred to as HT ss (high-temperature form of the $(Zn_xCu_{2-x})V_2O_7$ solid solution). The phase transition from LT ss to HT ss was sufficiently rapid in order to measure the XRD pattern, and several repeated measurements confirmed that the HT ss was stable. After holding for several hours at 973 K, the SEM-EDX analysis verified that the cooled samples were not contaminated by the Pt heating plate.

Brown and Hummel[13] reported only the diffraction pattern of β-$Zn_2V_2O_7$, which agreed well with our measurement for $x = 2$. By using a high-temperature precession camera, Gopal and Calvo analyzed that the crystallographic symmetry of β-$Zn_2V_2O_7$ was $C2/m$.[11] Our separate study[24] reports that the HT ss is a complete solid solution between γ-$Cu_2V_2O_7$ and β-$Zn_2V_2O_7$ with the symmetry of $C2/m$ by considering their thermal stability, and that α-$Cu_2V_2O_7$ is stable at a limited temperature and compositional range as shown in Fig. 4.

As shown in Fig. 1, α-$Cu_2V_2O_7$ (orthorhombic, F*dd2*) is as a type of a polymorphous modification of β-$Cu_2V_2O_7$. The VO_4 units were connected in a zigzag manner and they are commonly found in orthorhombic and monoclinic structures; a certain slight position shift and rotation of the VO_4 units causes a polymorphous transition between them. Although the detailed crystal structure of the HT ss has not been satisfactorily analyzed, γ-$Cu_2V_2O_7$ is expected to have a layered structure with V_2O_7 units similar with that of β-$Cu_2V_2O_7$. Because Zn atoms replace the Cu sites in the bipyramid of $(Cu,Zn)O_5$, the length of the *ab*-plane of the monoclinic lattice is modified.[9] This Zn replacement in the Cu sites stabilizes the monoclinic lattice, and the stable compositional regions of β- and γ-$Cu_2V_2O_7$ expand toward the Zn-rich region.

3.4 Thermoelectric properties

Figures 6(a) and (b) show the temperature dependence of α and ρ, respectively, of the studied samples. Because of the higher resistivity at lower temperatures, as shown in Fig. 6(b), it was difficult to measure α below 473 K.

The Seebeck coefficient of $Cu_2V_2O_7$ was about $-400\,\mu V/K$, showing the n-type thermoelectric property. For the LT ss, the larger negative values of α were measured for $0.2 \leq x \leq 1.0$. At higher temperatures, these values gradually approached toward zero.

The compositional behavior of α shows that DOS at the

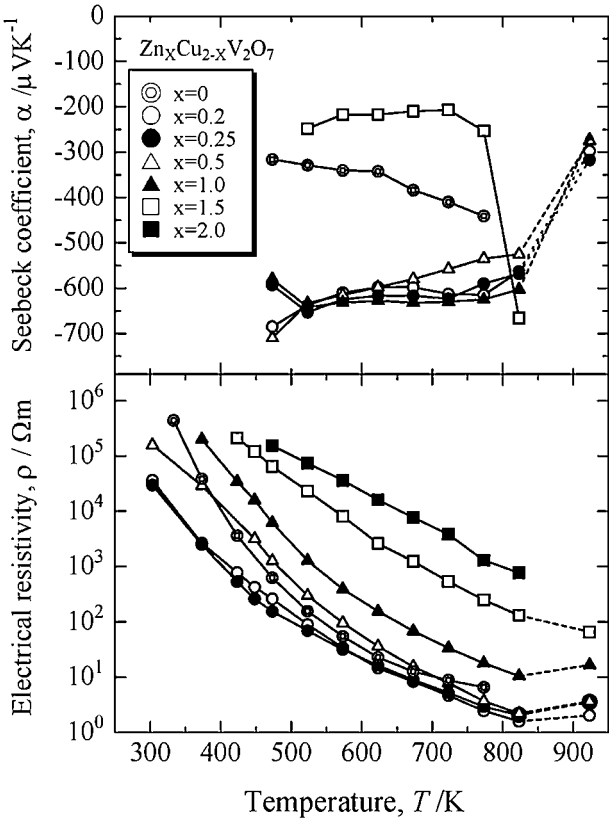

Fig. 6 Temperature dependence of α and ρ.

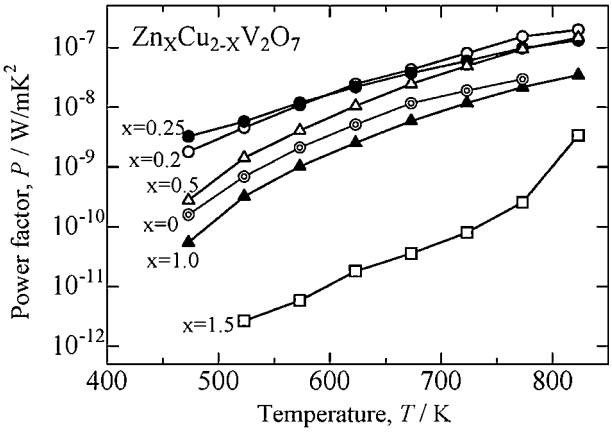

Fig. 7 Temperature dependence of P.

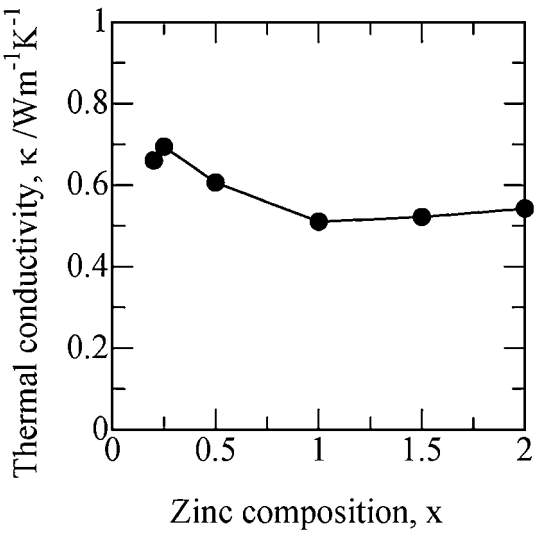

Fig. 8 Compositional dependency of κ.

Fermi level, which may influence the α value, does not shift monotonically with Zn addition. Especially the α value for the $x = 1.5$ sample exhibited an unusual temperature dependence as compared to the other samples. The DOS at the Fermi level has not been reported; this unusual behavior cannot be explained by a compositional change in the DOS. Because this sample exhibited a high electrical resistance (shown in Fig. 6(b)), an experimental error might be induced in α of $x = 1.5$ at the EMF measurement stage.

For the LT ss, the ρ value decreased when the samples were heated at higher temperatures, which appears to be a semiconductive behavior.

It should be noted that the α and ρ values at 923 K correspond to those for the HT ss at $0.2 \leq x \leq 1.0$. Evidently, these discontinuous behaviors can be attributed to the phase transition. For the HT ss, α was approximately $-300\,\mu V/K$, which is approximately half that for the LT ss. The resistivities for both LT ss and HT ss decreased as the zinc concentration x decreased.

Figure 7 shows the power factor deduced as $P = \alpha^2/\rho$. It increased with the temperature; it also increased when a larger amount of Cu was added. The P value was better for the LT ss than the HT ss. For the LT ss, P was maximum—$1.99 \times 10^{-7}\,W/m\,K^2$—at 823 K.

Figure 8 shows the thermal conductivity κ of the single phase of LT ss measured at room temperature. The values of κ are very low such as 0.6–0.8 mK/W. This indicates that the layered structure intercepts heat transfer through the pyramid structure of VO_4 and the metallic ion layer, as a characteristic feature of the layered oxides.

Assuming that the values of κ are constant against temperature and phase transformation, the non-dimensional figure of merit ZT was evaluated. The maximum value of ZT was 2.48×10^{-4} for LT ss at $x = 0.2$ and $T = 823$ K. Because α are as large as -520 to $-700\,\mu V/K$ and κ are $<1\,W/mK^2$, the improvement of electric conductivity as n-type conductor is desired, for example, by a modification in sample preparation or doping of the other elements.

4. Conclusion

The phase stability and thermoelectric properties of a layered structure of a $(Zn_xCu_{2-x})V_2O_7$ solid solution were studied for $x > 0.2$. XRD measurements, compositional studies, and DTA analysis verified that the low-temperature form of the $(Zn_xCu_{2-x})V_2O_7$ solid solution (LT ss, monoclinic structure, $C2/c$) was stable at $0.25 \leq x \leq 2$ when the sample was fabricated by solid-state sintering and subsequent annealing at 823 K in air. A high-temperature form of the $(Zn_xCu_{2-x})V_2O_7$ solid solution (HT ss) was formed at $0.2 \leq x \leq 2$. The phase transformation between the LT ss and HT ss occurred at a nearly constant temperature—approximately 873 K.

For the LT ss, α showed large negative values in the range of approximately -520 to $-700\,\mu V/K$ and ρ increased with Zn addition. κ at room temperature were as low as 0.6–0.8 mK/W. For the LT ss, P and ZT were the maximum at 823 K–$1.99 \times 10^{-7}\,W/mK^2$ and 2.48×10^{-4}, respectively, by neglecting temperature dependency of κ. The thermoelectric properties of the LT ss were better than those of the HT ss.

Acknowledgements

The authors would wish to thank Mr. T. Unesaki at Department of Material Science, Kyoto University, for assisting in the SEM-EDX analysis.

REFERENCES

1) I. Terasaki, Y. Sasago and K. Uchinokura: Phys. Rev. B **56** (1997) 12685.
2) C. Fouassier, G. Matejka, J.-M. Reau and P. Hagenmuller: J. Solid State Chem. **6** (1973) 532.
3) Y. Ono, R. Ishikawa, Y. Miyazaki, Y. Ishii, Y. Morii and T. Kajitani: J. Solid State Chem. **166** (2002) 177–181.
4) Y. Uchiyama, Y. Sasago, I. Tsukada, K. Uchinokura, A. Zheludev, T. Hayashi, N. Miura and P. Böni: Phys. Rev. Lett. **83** (1999) 632–635.
5) A. A. Salah, K. Benkhouja, K. Jaafari, J. Romero de Paz, E. Climent and R. Sáez Puche: J. Alloy Compd. **402** (2005) 213–218.
6) Z. He, Y. Ueda and M. Itoh: Solid State Comm. **141** (2007) 22–24.
7) D. Mercurio-Levand and B. Frit: Comp. Rend. Acad. Sci. (Paris) Ser. C **277** (1973) 1101–1104.
8) A. G. Nord and T. Stefanidis: Mater. Res. Bull. **20** (1985) 845–851.
9) M. Schindler and F. C. Hawthorne: J. Solid State Chem. **146** (1999) 271–276.
10) F. Larson and G. McCarthy: ICDD-JCPDS card #38-251 (1986).
11) R. Gopal and C. Calvo: Can. J. Chemistry **51** (1973) 1004–1009.
12) D. Mercurio-Levand and B. Frit: Acta Cryst. **B29** (1973) 2737–2741.
13) J. J. Brown and F. A. Hummel: Trans. Brit. Ceram. Soc. **64** (1965) 419–37.
14) P. Fleury: Comp. Rend. Acad. Sci. (Paris) Ser. C **263** (1966) 1375–1377.
15) K. Amezawa, Y. Kitajima, Y. Tomii and N. Yamamoto: Electrochem. Solid State Lett. **7** (2004) A511–A514.
16) K. Amezawa, Y. Nishikawa, Y. Tomii and N. Yamamoto: J. Electrochem. Soc. **152** (2005) A1060–A1067.
17) R. O. Suzuki, T. Ogawa and K. Ono: J. Amer. Ceram. Soc. **82** (1998) 2033–38.
18) R. O. Suzuki, T. Ogawa and R. Kondo: J. Amer. Ceram. Soc. (2006) in press.
19) T. Maruoka and R. O. Suzuki: Mater. Trans. **47** (2005) 1422–1427.
20) P. Galy: Bull. Soc. Chim. Fr. (1967) 261.
21) J. Angenault: Rev. Chim. Miner. **7** (1970) 651–699.
22) C. Calvo and R. Faggiani: Acta Cryst. **B31** (1975) 603–605.
23) C. M. Clark and R. Garlick: J. Inorg. Nucl. Chem. **40** (1978) 1347–1349.
24) K. Sotojima, R. O. Suzuki, K. Amezawa and Y. Tomii: J. Amer. Ceram. Soc., to be submitted.
25) Calculated pattern, filed as ICDD-JCPDS card #73-1032 (1997).